Research articles

Spin- and valley-dependent electronic band structure and electronic heat capacity of ferromagnetic silicene in the presence of strain, exchange field and Rashba spin-orbit coupling

Bui Dinh Hoi [a,b], Mohsen Yarmohammadi [c,*], Houshang Araghi Kazzaz [d]

[a] *Institute of Research and Development, Duy Tan University, K7/25 Quang Trung, Danang, Viet Nam*
[b] *Department of Physics, Hue University's College of Education, 34 Le Loi, Hue City, Viet Nam*
[c] *Young Researchers and Elite Club, Kermanshah Branch, Islamic Azad University, Kermanshah, Iran*
[d] *Department of Energy Engineering and Physics, Amirkabir University of Technology, Tehran, Iran*

ARTICLE INFO

ABSTRACT

We studied how the strain, induced exchange field and extrinsic Rashba spin-orbit coupling (RSOC) enhance the electronic band structure (EBS) and electronic heat capacity (EHC) of ferromagnetic silicene in presence of external electric field (EF) by using the Kane-Mele Hamiltonian, Dirac cone approximation and the Green's function approach. Particular attention is paid to investigate the EHC of spin-up and spin-down bands at Dirac K and K' points. We have varied the EF, strain, exchange field and RSOC to tune the energy of inter-band transitions and consequently EHC, leading to very promising features for future applications. Evaluation of EF exhibits three phases: Topological insulator (TI), valley-spin polarized metal (VSPM) and band insulator (BI) at given aforementioned parameters. As a new finding, we have found a quantum anomalous Hall phase in BI regime at strong RSOCs. Interestingly, the effective mass of carriers changes with strain, resulting in EHC behaviors. Here, exchange field has the same behavior with EF. Finally, we have confirmed the reported and expected symmetry results for both Dirac points and spins with the study of valley-dependent EHC.

1. Introduction

A puckered honeycomb geometry of silicon (Si) atoms, so-called silicene as a new massless Dirac fermion system has been attracted a great deal of attention both theoretically and experimentally [1–5]. The detectable quantum spin Hall effect is one of the results of its strong spin-orbit coupling (SOC) [6–9]. The possibility of dissipationless spin currents along its edges makes silicene useful for technological applications in spintronics field. Silicon atoms constitute the sp^2/sp^3 mixed hybridization while hybridization of carbon atoms in graphene is sp^2 [10]. The buckled structure plus the large ionic atomic volume of Si atoms lead to a large SOC which is roughly 1000 times larger than graphene [11,12]. On the other hand, the mixture hybridizations sit the A and B sublattices in different vertical planes with a separation of $d \approx 0.23$ Å [13,14], as shown in Fig. 1. Like graphene, the low-energy dynamics of carriers at two Dirac K and K' points of the hexagonal first Brillouin zone (FBZ) can be described well by massive Dirac theory because of

the mentioned above large SOC [15]. These features open a band gap in silicene band structure which is quoted as $\Delta_{SO} \approx 1.55-7.9$ meV from density functional theory and tight-binding calculations [6,8,13]. As a result, it is found that the Dirac nature of fermions leads to a TI phase in silicene. Also, it has been predicted that an on-site potential difference ($\Delta_z = E_z d$) can be created by applying an external EF, E_z, between sublattices, yielding a tunable band gap [13,14,16]. They have shown that the spin degeneracy at Dirac K and K' points can be broken with EF. For $\Delta_z > \Delta_{SO}$, a transition from TI to BI is reported [13,16]. At the critical value, $\Delta_z = \Delta_{SO}$, the lowest band gap at each valley closes, forming a Dirac-like point which is referred to a valley-spin-polarized metal (VSPM) phase.

Since the silicene band structure is tunable and may posses different phases by an external EF, it is worth study the spin-dependent phenomena, for example EHC. Moreover, a RSOC (or extrinsic SOC) term naturally also appears in the effective models for silicene by structural inversion asymmetry of the system by applying gate voltage, curvature and substrate effects [17–19]. Controlling SOC plays a key role for application of silicene-based structures in spintronics field [20–22]. However, this term has a

* Corresponding author.
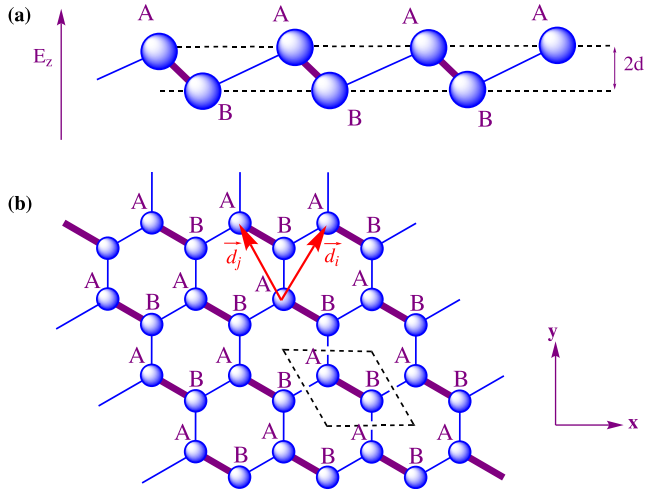*E-mail address:* m.yarmohammadi69@gmail.com (M. Yarmohammadi).

Fig. 1. (a) Side view and (b) top view schematic illustration of silicene sheet. The A and B sites separated by a distance $2d$ within the EF, E_z. The black dashed lines illustrate the Bravais unit cell including two atoms. $\vec{d}_i$ and $\vec{d}_j$ are two typical vectors connecting the next nearest neighbors.

negligible effect on the energy dispersion and could be neglected for most purposes [23,24] which is confirmed by our results. Beside electronic properties, thermal properties of silicence are still not well studied. Due to the specific lattice of monolayer silicene, investigation of thermal conductivity and thermodynamic properties are interesting. Many works have been done in this case, for example thermal conductivity of silicene is predicted around 20–65 W/mK in Refs. [25–29]. EHC of a semiconductor system is defined as the ratio of heat used by the carriers (here, Dirac fermions) to the rise in temperature of the system [30]. Our system is considered as a ferromagnetic with an exchange field M. In order to induce ferromagnetic correlation in graphene and silicene, a metallic ferromagnetic material is used as substrate [31].

In real electronic circuits based on the low-dimensional systems, the systems have been fixed with an intrinsic strain and stress strengths. The strain can change many features of 2D-materials. In graphene, Dirac points remain at K and K' valleys under biaxial strain, but they affected for strain along the different directions [32–35]. Contrary to the graphene, both σ^* and π^* bands in silicene are more sensitive to the strain-induced [36–40]. For example, silicene becomes metallic under biaxial strain larger than 12% [36–38] and it turns into a metal under stain larger than 12% (14%) along the armchair (zigzag) directions [40]. However, the

dependent EBS and EHC. In Section 4 the numerical results are explained. Conclusions are given in Section 5.

2. The effective Hamiltonian model and Green's functions

Here is considered a monolayer silicene system on the *xy*-plane, exposed to the perpendicular EF, E_z, as illustrated in Fig. 1. The system is described by following model in order to study the dynamics of carriers [41]

$$
\begin{aligned}
H = &-t_0 \sum_{\langle i,j \rangle,\sigma} c_{i,\sigma}^\dagger c_{j,\sigma} + \mathrm{i}\frac{\Delta_{SO}}{3\sqrt{3}} \sum_{\ll i,j \gg,\sigma,\sigma'} v_{ij} c_{i,\sigma}^\dagger \sigma_z^{\sigma,\sigma'} c_{j,\sigma'} \\
&+ \mathrm{i}\sum_{i,j,\sigma,\sigma'} c_{i,\sigma}^\dagger (\vec{u}_{ij}\cdot\vec{\sigma})_{\sigma,\sigma'} c_{j,\sigma'} + d\sum_{i,\sigma}\varsigma_i E_z^i c_{i,\sigma}^\dagger c_{i,\sigma} \\
&+ \sum_{i,\sigma} M_i \sigma_z c_{i,\sigma}^\dagger c_{i,\sigma} + h.c.,
\end{aligned}
\tag{1}
$$

in which the first term denotes the nearest-neighbor hopping with energy of $t_0 \simeq 1.3$ *eV* and the sum runs over all neighboring pairs $\langle i,j \rangle$. $c_{i,\sigma}^\dagger (c_{i,\sigma})$ creates (annihilates) an electron with spin-up and spin-down as σ_z at site i. The first two terms illustrate the Kane-Mele Hamiltonian describing the SOC with $\Delta_{SO} \simeq 1.55$ *meV*, being $\vec{\sigma} = (\sigma_x, \sigma_y, \sigma_z)$ the Pauli matrices. Also is defined $v_{ij} = \frac{(\vec{d}_i \times \vec{d}_j)\cdot\hat{z}}{|(\vec{d}_i \times \vec{d}_j)\cdot\hat{z}|} = \pm 1$, with $\vec{d}_i$ and $\vec{d}_j$ being the two typical vectors which connect the next nearest neighbors, and sum over all such pairs indicated by $\ll i,j \gg$ [42,43]. $\vec{u}_{ij} = -(\Delta_R/a_0)\hat{z}\times\vec{\delta}_{ij}$ which $|\vec{\delta}_{ij}| = a_0$ is the length of the lattice translational vector, Δ_R is the normalized magnitude of RSOC [44]. The fourth term is the staggered sublattice potential term as mentioned before in Section 1 with $\varsigma_i = +1(-1)$ for $A(B)$ sites. The final term is related to the induced exchange magnetic field by the magnetic insulator substrate. The effect of strain on Hamiltonian is given by the two-dimensional reductions of the strain tensor as follows [35,45]

$$
\varepsilon = \epsilon\begin{pmatrix} \cos^2\theta - v\sin^2\theta & (1+v)\cos\theta\sin\theta \\ (1+v)\cos\theta\sin\theta & \sin^2\theta - v\cos^2\theta \end{pmatrix},
\tag{2}
$$

In this equation, θ denotes the angle which the applied strain with respect to the x axis direction, ϵ is the strain modulus and $v = 0.62$ is Poisson's ratio from *ab initio* calculations for silicene [46]. In our calculations $\theta = 0$ refers to strain along the zigzag direction. Therefore, we have considered our calculations based on the strain-induced and converted nearest neighbors vectors. The low-energy limit of the above Hamiltonian in a ferromagnetic silicene in presence of a perpendicular uniform EF is described as [6,8,23]:

$$
\begin{aligned}
H_{\eta,\sigma_z}^0 &= \hbar v_F(k_x \tau_x - \eta k_y \tau_y) - \eta\Delta_{SO}\tau_z\sigma_z + \eta a\lambda_R\tau_z(k_x\sigma_y - k_y\sigma_x) + \Delta_z\tau_z - M\sigma_z \\
&= \begin{pmatrix} \Delta_z - \eta\Delta_{SO} - M & \eta a\lambda_R(-k_y - ik_x) & \hbar v_F(k_x + i\eta k_y) & 0 \\ \eta a\lambda_R(-k_y + ik_x) & \Delta_z + \eta\sigma_z\Delta_{SO} - M & 0 & \hbar v_F(k_x + i\eta k_y) \\ \hbar v_F(k_x - i\eta k_y) & 0 & -\Delta_z + \eta\Delta_{SO} + M & -\eta a\lambda_R(-k_y - ik_x) \\ 0 & \hbar v_F(k_x - i\eta k_y) & -\eta a\lambda_R(-k_y + ik_x) & -\Delta_z - \eta\Delta_{SO} + M \end{pmatrix},
\end{aligned}
\tag{3}
$$

investigation of thermodynamic properties of silicence under strain is still remain to be studied.

In this work, we have investigated the effects of strain, EF, exchange field and RSOC on band structure and EHC of a ferromagnetic silicene in three mentioned phases at Dirac points. Green's function approach is carried out with the Kane-Mele Hamiltonian to study the dynamics of massive carriers. The outline of this paper is as follows: Section 2 describes the Hamiltonian and calculation details. Section 3 shows the calculated spin- and valley-

wherein v_F is the Fermi velocity of carriers for the in-plane momentum $\mathbf{k} = (k_x, k_y)$ of the FBZ. $a \approx 3.86$ Å is the equilibrium lattice constant of silicene and $\tau_i(i = x, y, z)$ are the Pauli matrices in the sublattice space. The first term in Eq. (1) is the pristine graphene Hamiltonian at Dirac cone approximation for $K(K')$ points indexed by $\eta = +1(-1)$. This term refers to the intra-layer hopping from A atoms to B atoms and vice versa. The second term is the Kane-Mele Hamiltonian for the intrinsic SOC [6,47]. If silicene rests

onto the surface of a magnetic insulator or metallic ferromagnetic substrate, an exchange magnetization field can be induced as $M = \Delta_{SO}/2$ [48,49]. The Hamiltonian after strain is given by

$$H^0_{\tau,s_z} = \begin{pmatrix} \frac{1}{2}\Delta_z + \frac{1}{2}\eta\sigma_z\Delta_{SO} - M\sigma_z & \eta a\Delta_R(k'_y + ik'_x) & \hbar v_F(\eta k'_x - ik'_y) & 0 \\ \eta a\Delta_R(k'_y - ik'_x) & \frac{1}{2}\Delta_z - \frac{1}{2}\eta\sigma_z\Delta_{SO} - M\sigma_z & 0 & \hbar v_F(\eta k'_x - ik'_y) \\ \hbar v_F(\eta k'_x + ik'_y) & 0 & -\frac{1}{2}\Delta_z - \frac{1}{2}\eta\sigma_z\Delta_{SO} + M\sigma_z & -\eta a\Delta_R(k'_y + ik'_x) \\ 0 & \hbar v_F(\eta k'_x + ik'_y) & -\eta a\Delta_R(k'_y - ik'_x) & -\frac{1}{2}\Delta_z + \frac{1}{2}\eta\sigma_z\Delta_{SO} + M\sigma_z \end{pmatrix}, \quad (4)$$

with $k'_x = k_x(1 - \lambda_x\epsilon)$ and $k'_y = k_y(1 - \lambda_y\epsilon)$ where $\lambda_x = 2.2$ and $\lambda_y = -1.3$ are the logarithmic derivative of the nearest-neighbor hopping with respect to the lattice parameter ($a = 3.86$ Å) at $\epsilon = 0$ along the x and y directions, respectively [50]. The Green's function matrix can be readily obtained by following equation

$$\mathbf{G}^{-1}_{\eta,\sigma_z}(\mathbf{k}, i\omega_n) = i\omega_n\hat{\mathbf{I}} - H_{\eta,\sigma_z}(\mathbf{k}). \quad (5)$$

Having substituted Eq. (4) into Eq. (5), the explicit form of the Green's function matrix is found but has not been written here because it is quite lengthy.

3. Spin- and valley-dependent energy dispersion and electronic heat capacity

DOS can be calculated by the trace of imaginary part of the Green's function matrix, $D(\varepsilon) = -\Im TrG(\varepsilon)/\pi$ [50]. Taking trace over the quantum numbers which label the Hamiltonian, engaging Eqs. (1) and (5) along with setting $i\omega_n \rightarrow \varepsilon + i0^+$ as an analytical continuation (being 0^+ a very small real number), the total DOS would be eventuated

$$D_{\eta,\sigma_z}(\varepsilon) = -\frac{1}{\pi N_c}\sum_{\mu,\mathbf{k}}\Im G^{\mu\mu}_{\eta,\sigma_z}(\mathbf{k}, \varepsilon + i0^+), \quad (6)$$

where μ describes a sub-site and N_c is the number of unit cells (or the number of $\mathbf{k}$ vectors in the FBZ). Although DOS of the system has been calculated and utilized in extraction of EHC, its graphs are not presented here; instead we have studied the electronic structure by means of the eigenvalues $\varepsilon(\mathbf{k})$ of Eq. (4) which give the EBS as

$$\varepsilon_{\eta,\sigma_z}(\mathbf{k}) = \pm\frac{1}{2}$$

$$\times \sqrt{4\hbar^2 v_F^2 \mathbf{k}'^2 + \eta\left((\Delta_z - 2M\sigma_z) \pm \sqrt{4a^2\mathbf{k}'^2\Delta_R^2 + \Delta_{SO}^2}\right)^2} \quad (7)$$

In fact, DOS and EBS have the same meaning for studying the band gaps. The EHC could be introduced by following expression [51]
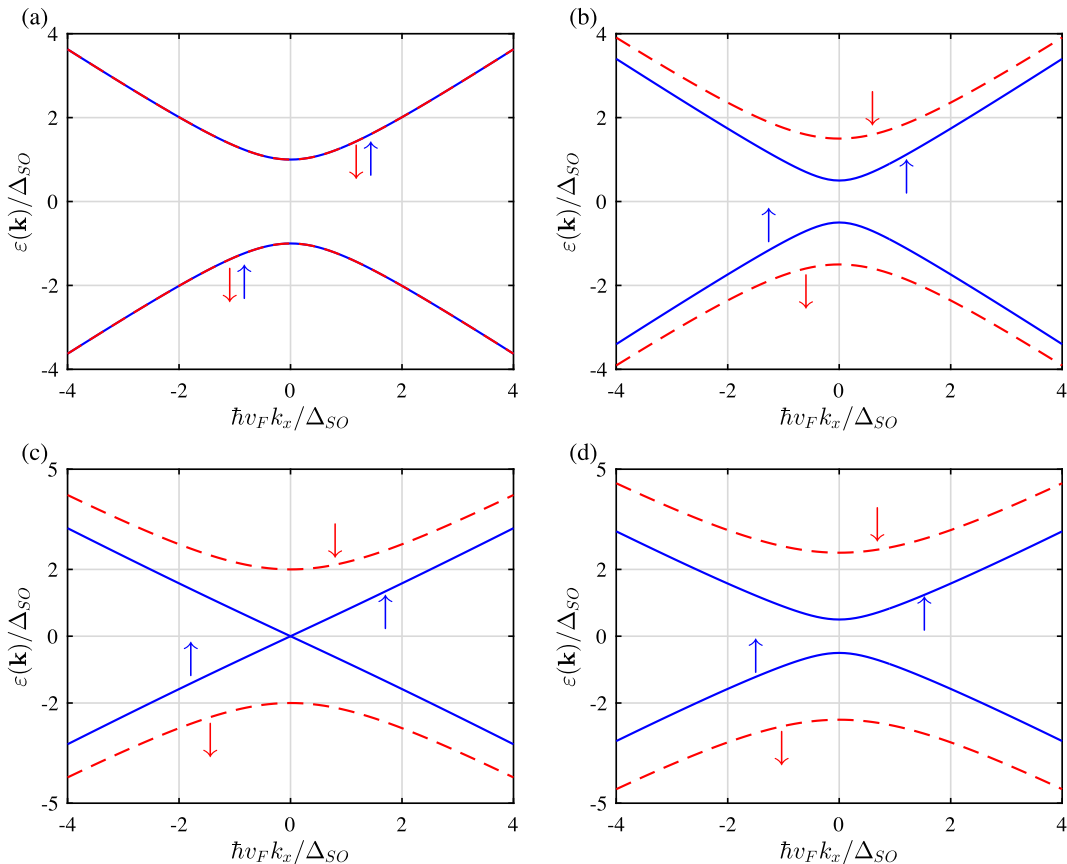

(a) (b) (c) (d)

Fig. 2. Spin-dependent electronic band structure of ferromagnetic silicene with $M = \Delta_{SO}/2$, $\Delta_R = \Delta_{SO}/2$ and $\epsilon = 10\%$ in valley K at (a) $\Delta_z/\Delta_{SO} = 0$ (TI regime), (b) $\Delta_z/\Delta_{SO} = 0.5$ (TI regime), (c) $\Delta_z/\Delta_{SO} = 1$ (VSPM regime) and (d) $\Delta_z/\Delta_{SO} = 1.5$ (BI regime).

$$C(T) = \int_{-\infty}^{+\infty} d\varepsilon \varepsilon D(\varepsilon) \partial_T f(\varepsilon) \qquad (8)$$

in which $D(\varepsilon)$ calculated by Eq. (6) and $f(\varepsilon) = 1/[e^{\varepsilon/k_B T} + 1]$ (k_B is the Boltzmann constant) represents the Fermi–Dirac distribution function. By using Eqs. (6) and (8), the EHC would be obtained as

$$C_{\eta,\sigma_z}(T) = -\frac{1}{\pi N_c T^2} \sum_{\mu,\mathbf{k}} \Im \int_{-\infty}^{+\infty} d\varepsilon \frac{\varepsilon^2 e^{\varepsilon/k_B T}}{(e^{\varepsilon/k_B T} + 1)^2} G_{\eta,\sigma_z}^{\mu\mu}(\mathbf{k}, \varepsilon + i0^+) \qquad (9)$$

4. Numerical results and discussions

In this section, taking into account Eqs. (4), (5), (7) and (9), we obtain the entire low-energy EHC and MS curves. Also, we have completed our analytical calculations based on the reported parameters in Ref. [8]. Here, results are at K point and at K' point, the spin labels only switch, as shown in Figs. 10 and 11.

The reproduced results of Ref. [44] for EBS evolution with Δ_z in the presence of strain, RSOC and exchange field is shown in Fig. 2. When $\Delta_z = 0$, a spin degeneracy appears which energy bands are separated by an insulating gap of $2\Delta_{SO}$ and the system is in the TI regime. For $\Delta_z < \Delta_{SO}$, system remains at TI phase with a spin splitting and two energy gaps ($|\Delta_{k,\uparrow}|$ and $|\Delta_{k,\downarrow}|$) which $|\Delta_{k,\uparrow}| < |\Delta_{k,\downarrow}|$. In this regime (TI), the spin-up (down) energy gap decreases (increases) with Δ_z. At $\Delta_z = \Delta_{SO}$, the spin-up energy gap closes and then reopens by increasing Δ_z further ($\Delta_z > \Delta_{SO}$). As we mentioned before, $\Delta_z = \Delta_{SO}$ is corresponding value of electric field in VSPM regime. For $\Delta_z > \Delta_{SO}$, the system transitions to the BI regime and both gaps increase with Δ_z. All presented results are in agreement with Ref. [44].

It is well-known that EHC of semiconductors at low temperatures, can be written as $C(T) \propto e^{-\Delta/k_B T}$ [51,30,52]. The Schottky anomaly as an interesting effect can be explained with the change of entropy of the system. As we know, at zero temperature only the lowest energy level is occupied and entropy is zero. In this regards, there is a very little probability of a transition to a higher energy level but as the temperature increases, entropy increases and therefore the probability of a transition goes up. As the temperature closes to the difference between the energy levels in the system, there is a broad peak corresponding to a large change in entropy for a small change in temperature. At high temperatures, all levels are occupied and there is again a little change in entropy for small changes in temperature and thus a lower EHC [53]. Here, Δ is the combined electric field and RSOC potentials.

The corresponding curves for EHC in TI, VSPM and BI regimes are presented in Fig. 3. The total EHC at $\Delta_z = 0$ is 2 times larger than each spin which is reasonable because of the absence of EF. Also, the $T_{Schottky}$ ($\simeq \Delta_{SO}/k_B$) is constant for total and each spin in panel (a). The reason of how the heat capacity be tuned by EF is related to the band gap sizes in Fig. 2 based on the Eq. (9). By decreasing (increasing) the band gaps, EHC moves towards the lower (higher) temperatures due to the relation $C(T) \propto e^{-\Delta/k_B T}$. For all regimes, spin-down has the larger EHC than spin-up and $T_{Schottky}|_{spin-up} < T_{Schottky}|_{spin-down}$ because of the corresponding energy gaps. It is necessary to mention that for all regimes, total EHC is bigger than each spin.

Presented in Fig. 4 are the EBS for various strains which one can see that the strain does not affect the band gap size in the presence of $\Delta_z = \Delta_{SO}$ and $\Delta_R = \Delta_{SO}/2$ with VSPM phase. The remarkable point in these figures is the slope of curves which is obviousable by the initial value of $\varepsilon(\mathbf{k})/\Delta_{SO}$ at $\hbar v_F k_x/\Delta_{SO} = -4$. We have found that the
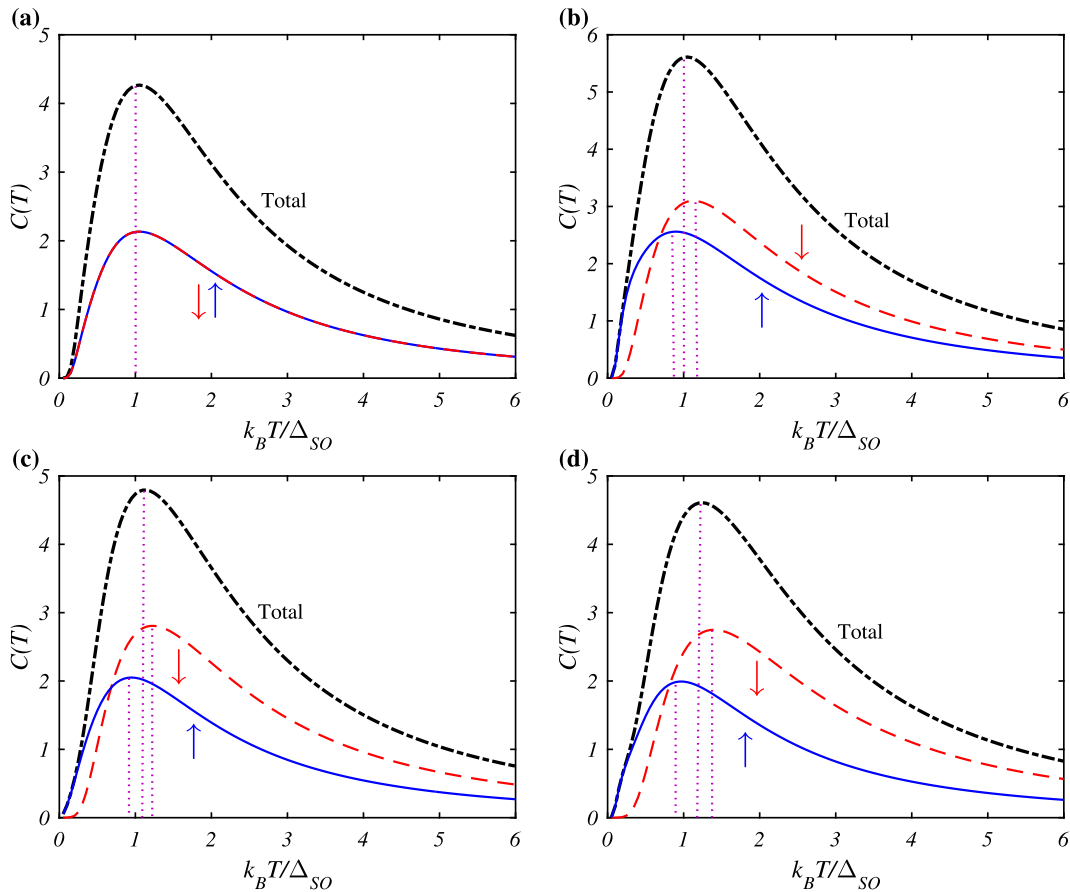

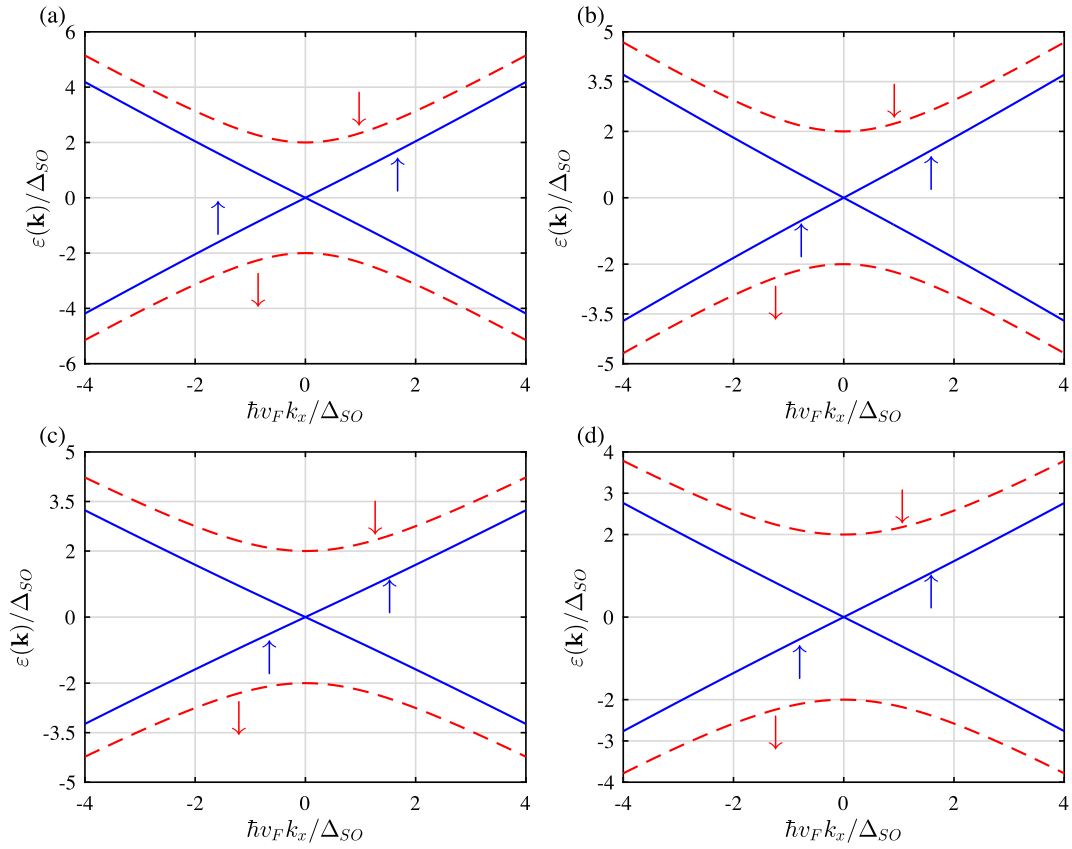**Fig. 3.** As Fig. 2 but for electronic heat capacity.

Fig. 4. Spin-dependent electronic band structure of ferromagnetic silicene with $M = \Delta_{SO}/2$, $\Delta_R = \Delta_{SO}/2$ and $\Delta_z = \Delta_{SO}$ in valley K at (a) $\epsilon = 0\%$, (b) $\epsilon = 5\%$, (c) $\epsilon = 10\%$ and (d) $\epsilon = 15\%$.
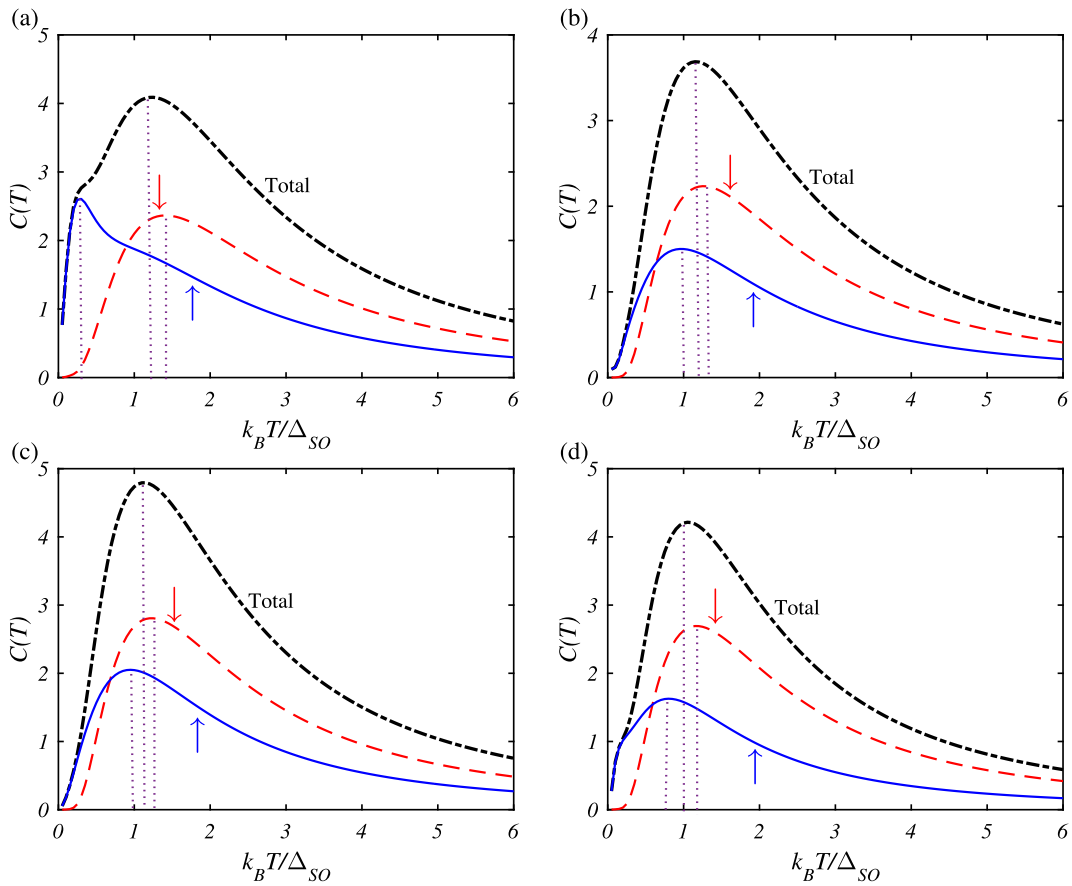

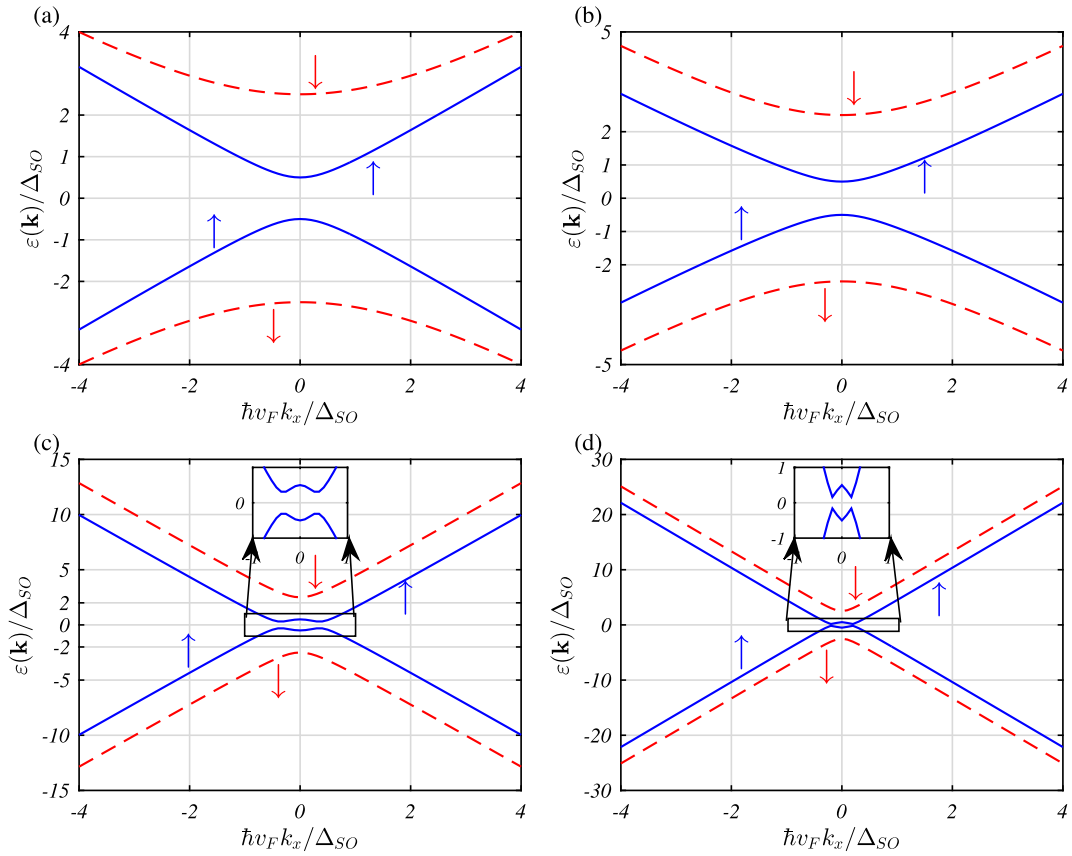**Fig. 5.** As Fig. 4 but for electronic heat capacity.

Fig. 6. Spin-dependent electronic band structure of ferromagnetic silicene with $M = \Delta_{SO}/2$, $\epsilon = 10\%$ and $\Delta_z = \frac{3}{2}\Delta_{SO}$ in valley K at (a) $\Delta_R = 0$, (b) $\Delta_R = \Delta_{SO}/2$, (c) $\Delta_R = \frac{3}{2}\Delta_{SO}$ and (d) $\Delta_R = \frac{15}{2}\Delta_{SO}$.
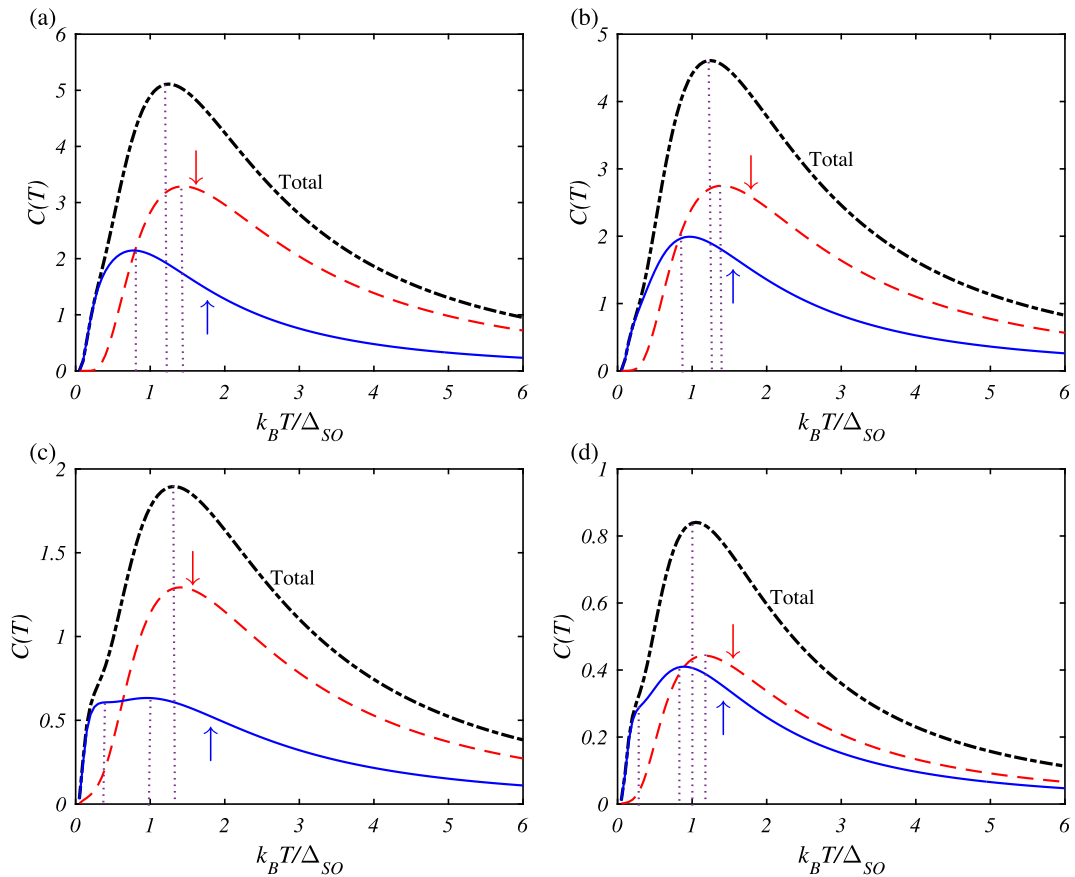

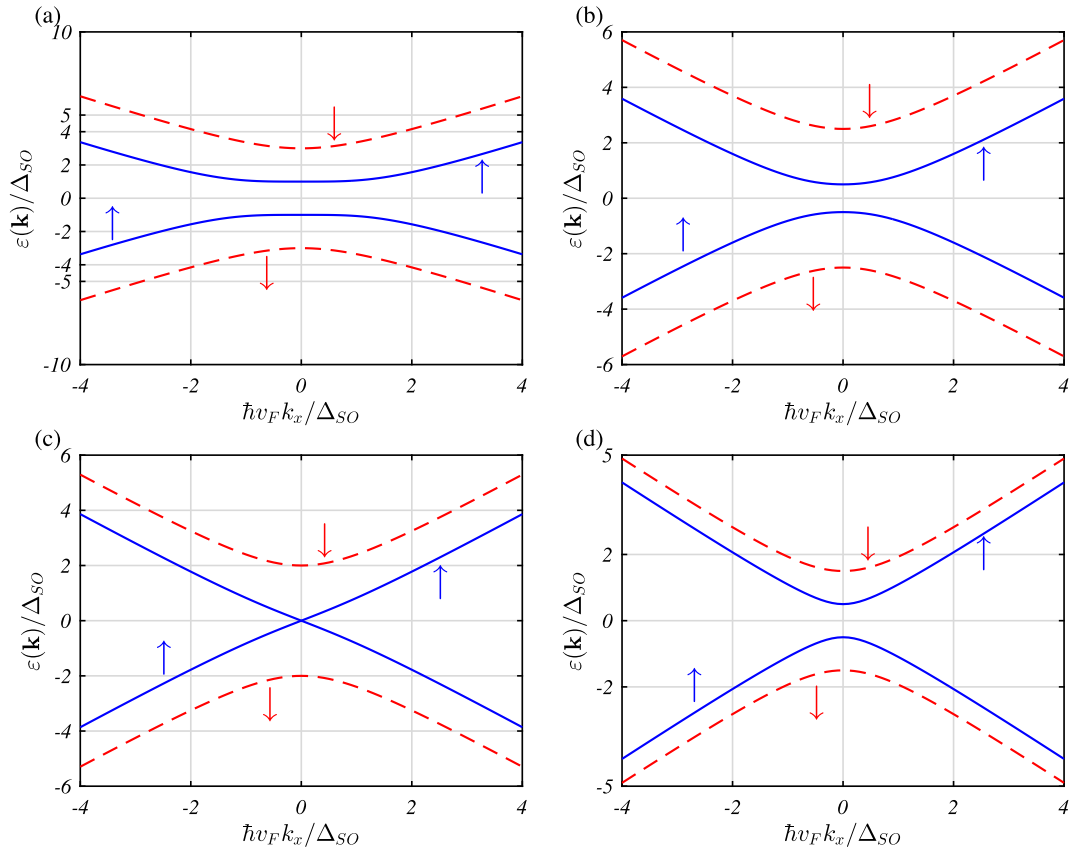**Fig. 7.** Similar to Fig. 6 but for electronic heat capacity.

Fig. 8. Spin-dependent electronic band structure of ferromagnetic silicene with $\Delta_R = \Delta_{SO}, \epsilon = 10\%$ and $\Delta_z = \frac{3}{2}\Delta_{SO}$ in valley K at (a) $M = 0$, (b) $M = \Delta_{SO}/2$, (c) $M = \Delta_{SO}$ and (d) $M = \frac{3}{2}\Delta_{SO}$.
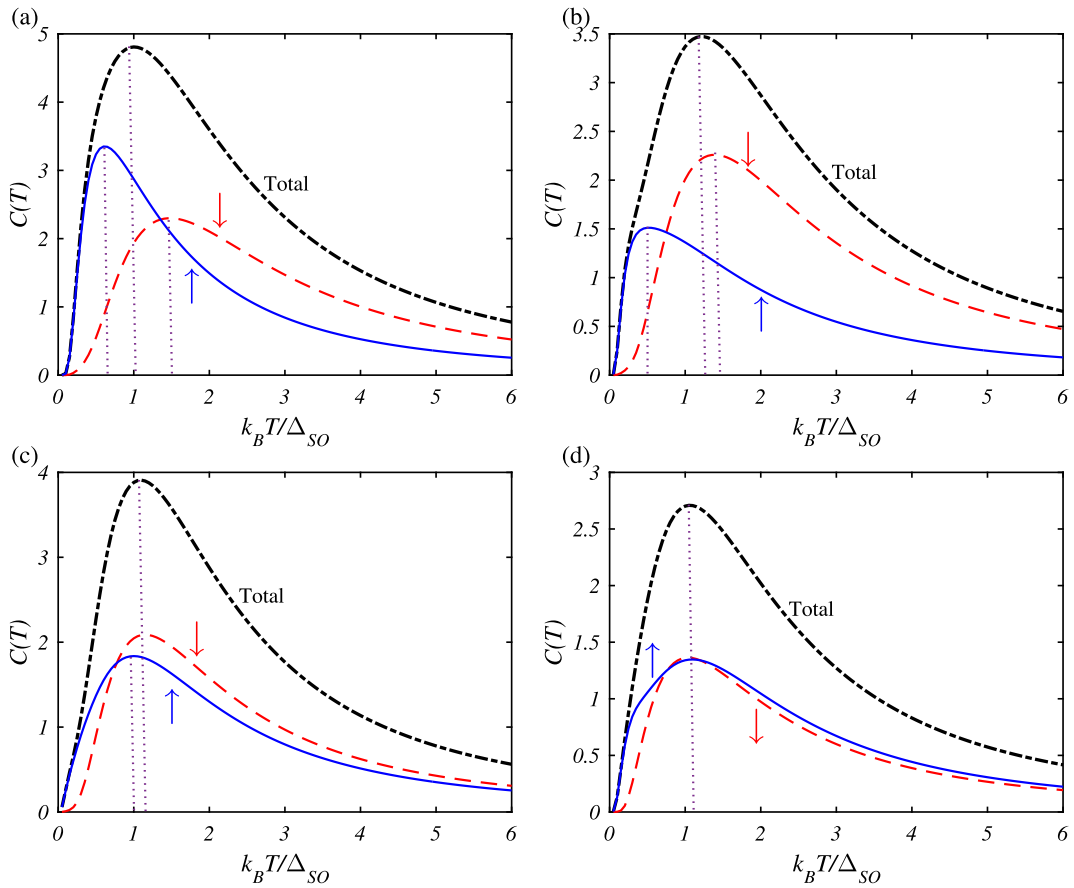

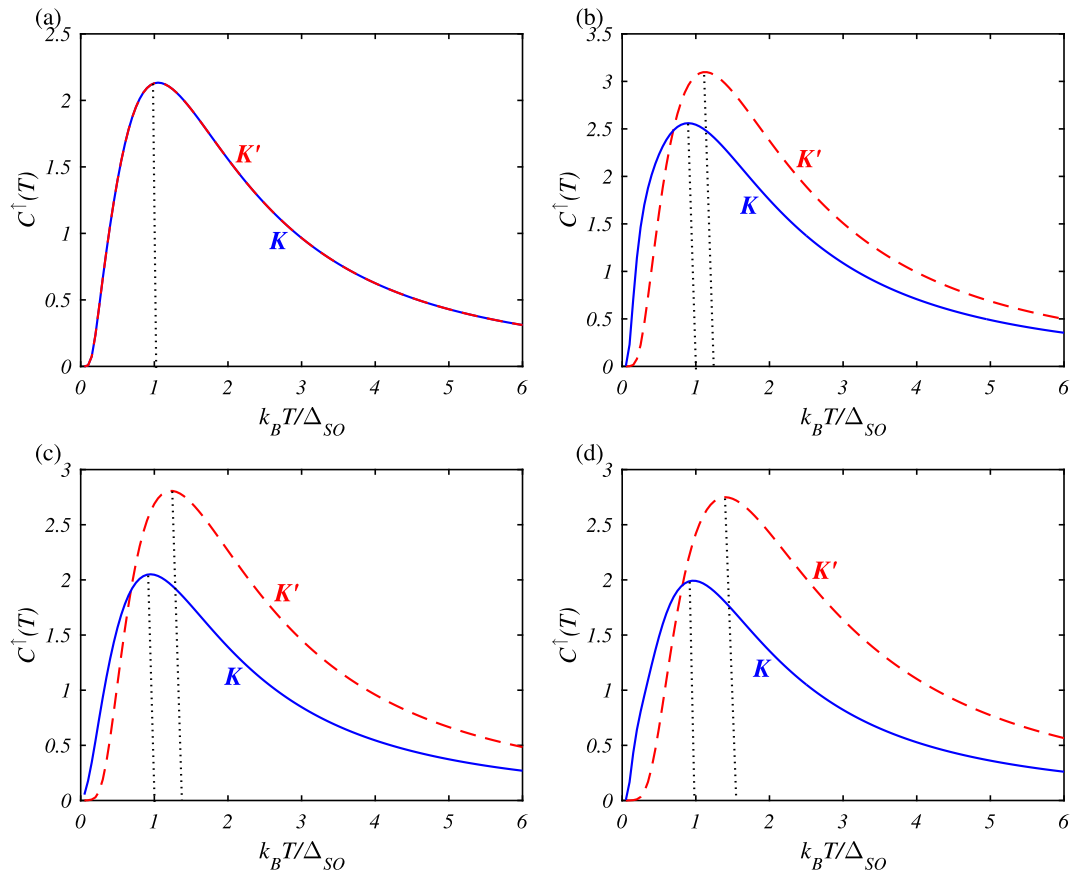**Fig. 9.** Fig. 8 but for electronic heat capacity.

Fig. 10. Valley-dependent electronic heat capacity of spin-up with $M = \Delta_{SO}/2, \Delta_R = \Delta_{SO}/2$ and $\epsilon = 10\%$ at (a) $\Delta_z/\Delta_{SO} = 0$ (TI regime), (b) $\Delta_z/\Delta_{SO} = 0.5$ (TI regime), (c) $\Delta_z/\Delta_{SO} = 1$ (VSPM regime) and (d) $\Delta_z/\Delta_{SO} = 1.5$ (BI regime).

slope of curves decreases with strain within the used model in Eq. (4). According to the concept of effective mass $(m^* = \hbar^2(\partial\varepsilon(\mathbf{k})/\partial\mathbf{k})^{-1})$, we can claim that the effective mass of carriers increases with strain, as soon as the band gap slope decreases. This creates a problem in the carriers's conductance. For this reason, EHC behavior changes with strain without the change of gaps. It is necessary to mention that, we had the slopes changes in the previous case (Fig. 2) but the band gap changes were more dominant than the effective mass. It is easy to understand the behavior of Schottky anomaly in Fig. 5. Evaluation of strain with small values leads to the increase of $T_{Schottky}$ for each spin because electrons need to the higher thermal energy to jump the band gap, but system turns into another state under strain larger than 10% in agreement with Ref. [40]. Factually, the scattering rate scale is the main reason of these behaviors. At large strains, carriers scatter from each other similar to the presence of a perturbation and goes to their initial state with more degree of freedom in transport.

The effects of RSOC on EBS and EHC of case $\Delta_z = \frac{3}{2}\Delta_{SO}$ have been studied in Figs. 6 and 7. One can see that the RSOC does not change the energy gaps effectively and only the slope of curves increases in agreement with Refs. [23,24]. We know that the slope of curves in band structures are responsible for the effective mass of carriers. By increasing the RSOC, slopes increase, leading to the reduction of effective masses. So, one can expect a decline behavior for $T_{Schottky}$ which a little shifting is observed. The total, spin-up and spin-down EHC slightly decreases with Δ_R up to Δ_{SO}. For $\Delta_R > \Delta_{SO}$, the EHC decreases more than $\Delta_R < \Delta_{SO}$ case. There is an interesting

behavior for $\Delta_R > \Delta_{SO}$ in the BI regime ($\Delta_z = \frac{3}{2}\Delta_{SO}$) and spin-up case. As a new finding, we have two direct band gaps around $k_x = 0$ symmetrically which leads to a quantum fluctuation in the system. For this reason, we witness a small fluctuation in spin-up EHC curve for $\Delta_R > \Delta_{SO}$. However, it affects the total EHC because of the difference between two spins.

Finally, we have investigated the spin-dependent EBS and temperature-dependent EHC in Figs. 7 and 8 for various exchange field strengths, namely $M = 0, M = \Delta_{SO}/2, M = \Delta_{SO}$ and $M = \frac{3}{2}\Delta_{SO}$. Surprisingly, both spin band gaps decrease with exchange field up to Δ_{SO} in $\Delta_z = \frac{3}{2}\Delta_{SO}, \Delta_R = \Delta_{SO}$ and $\epsilon = 10\%$. At $M = \Delta_{SO}$, spin-up band gap closes and then reopens for $M > \Delta_{SO}$ while spin-down band gap decreases still slightly. Exchange field and electric field have the same behaviors with a difference between the spin-down band gaps in $\Delta_z > \Delta_{SO}$ and $M > \Delta_{SO}$. The corresponding EHC curves show the reduction behavior for $T_{Schottky}$ of each spin with M up to Δ_{SO}. At $M = \Delta_{SO}$, required $T_{Schottky}$ to jump the gap energy is Δ_{SO}/k_B and increases for $M > \Delta_{SO}$ (see Fig. 9).

The valley-dependent EHC for spin-up and spin-down has been studied in Figs. 10 and 11, respectively with $M = \Delta_{SO}/2, \Delta_R/\Delta_{SO}/2$ and $\epsilon = 10\%$ at TI, VSPM and BI regimes. One can confirm the reported and expected symmetry aspects of Dirac K and K' points with the spin-up and spin-down cases [54]. For spin-up and $\Delta_z < \Delta_{SO}$, EHC at Dirac K' point is larger than Dirac K point which we expect the inverse reactions for spin-down (panel (b) in Fig. 11).
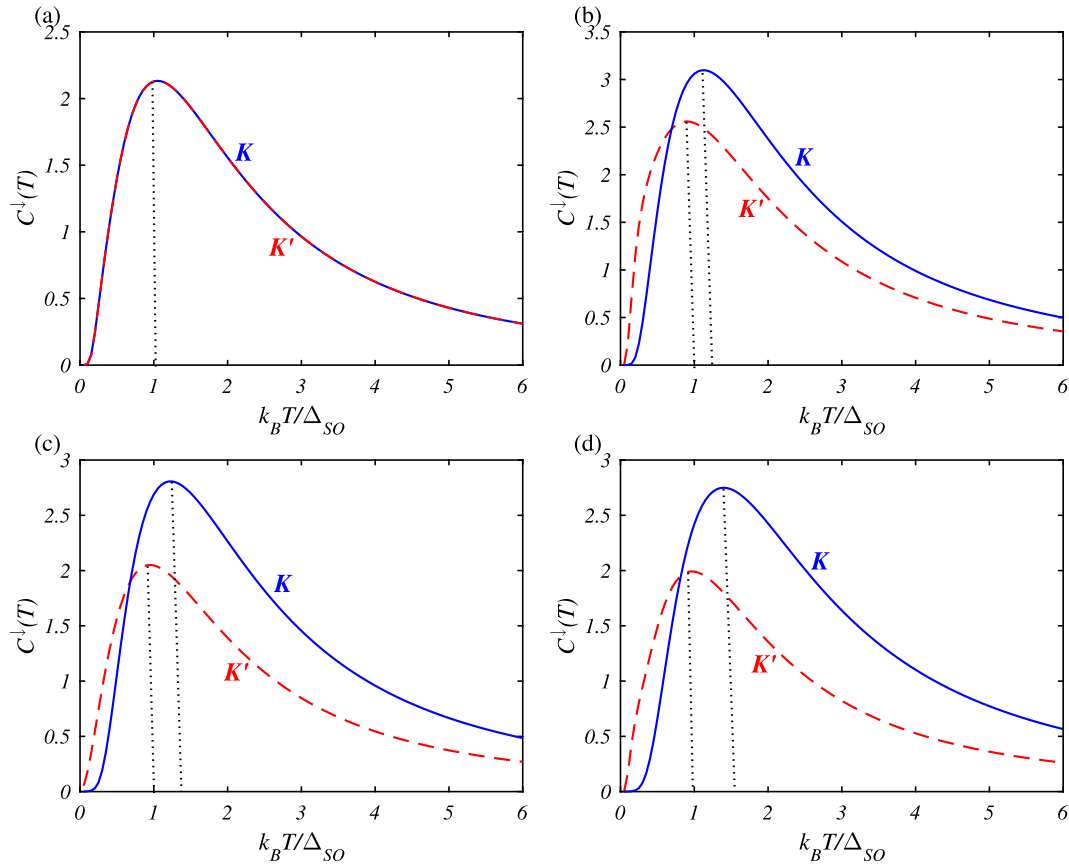
Fig. 11. Valley-dependent electronic heat capacity of spin-down with $M = \Delta_{SO}/2, \Delta_R = \Delta_{SO}/2$ and $\epsilon = 10$ % at (a) $\Delta_z/\Delta_{SO} = 0$ (TI regime), (b) $\Delta_z/\Delta_{SO} = 0.5$ (TI regime), (c) $\Delta_z/\Delta_{SO} = 1$ (VSPM regime) and (d) $\Delta_z/\Delta_{SO} = 1.5$ (BI regime).

5. Conclusions

To sum up, we have addressed the spin- and valley-dependent electronic band structure and electronic heat capacity of ferromagnetic silicene in three regimes including topological insulator, valley-spin polarized metal and band insulator in the presence of strain, exchange field, electric field and Rashba spin-orbit coupling. Our findings show that the electric field (strain) and exchange field (Rashba spin-orbit coupling) have the same behaviors in their bands. We have found an anomalous quantum spin Hall phase at strong Rashba spin-orbit couplings. Also, we have confirmed the symmetry aspects with the help of valley-dependent electronic heat capacity. Finally, we have varied the EF, strain, exchange field and RSOC to tune the energy of inter-band transitions and consequently EHC, leading to very promising features for future applications.

References

[1] B. Lalmi, H. Oughaddou, H. Enriquez, A. Kara, S. Vizzini, B. Ealet, B. Aufray, Appl. Phys. Lett. 97 (2010) 223109.
[2] F. Bao-Jie, Li Wen-Bin, Q. Jing-Lan, C. Peng, C. Lan, W. Ke-Hui, Chin. Phys. Lett. 32 (2015) 037302.
[3] P. De Padova, C. Quaresima, C. Ottaviani, P.M. Sheverdyaeva, P. Moras, C. Carbone, D. Topwal, B. Olivieri, A. Kara, H. Oughaddou, et al., Appl. Phys. Lett. 96 (2010) 261905.
[4] S. Cahangirov, M. Topsakal, E. Akturk, H. Sahin, S. Ciraci, Phys. Rev. Lett. 102 (2009) 236804.
[5] Y. Ding, J. Ni, Appl. Phys. Lett. 95 (2009) 083115.
[6] C.C. Liu, W. Feng, Y.G. Yao, Phys. Rev. Lett. 107 (2011) 076802.
[7] S. Cahangirov, M. Topsakal, E. Akturk, H. Sahin, S. Ciraci, Phys. Rev. Lett. 102 (2009) 236804.
[8] C.C. Liu, H. Jiang, Y.G. Yao, Phys. Rev. B 84 (2011) 195430.
[9] G.G. Guzman-Verri, L.C. Lew Yan Voon, Phys. Rev. B 76 (2007) 075131.
[10] L. Chen, H. Li, B. Feng, Z. Ding, J. Qiu, P. Cheng, K. Wu, S. Meng, Phys. Rev. Lett. 110 (2013) 085504.
[11] H. Min, J.E. Hill, N.A. Sinitsyn, B.R. Sahu, L. Kleinman, A.H. MacDonald, Phys. Rev. B 74 (2006) 165310.
[12] Y. Yao, F. Ye, X.-L. Qi, S.-C. Zhang, Z. Fang, Phys. Rev. B 75 (2007) 041401(R).
[13] N.D. Drummond, V. Zolyomi, V.I. Falko, Phys. Rev. B 85 (2012) 075423.
[14] Z. Ni, Q. Liu, K. Tang, J. Zheng, J. Zhou, R. Qin, Z. Gao, D. Yu, J. Lu, Nano Lett. 12 (2012) 113.
[15] S. Konschuh, M. Gmitra, J. Fabian, Phys. Rev. B 82 (2010) 245412.
[16] M. Ezawa, New J. Phys. 14 (2012) 033003.
[17] C. Bai, J. Wang, S. Jia, Y. Yang, Physica E 43 (2011) 884.
[18] A. Yamakage, K.-I. Imura, J. Cayssol, Y. Kuramoto, EPL. 87 (2009) 47005.
[19] N. Tombros, C. Jozsa, M. Popinciuc, H.T. Jonkman, B.J. van Wees, Nature (London) 448 (2007) 571.
[20] Y.A. Bychkov, E.I. Rashba, J. Phys. C 17 (1984) 6039.
[21] H. Zhang et al., Phys. Rev. Lett. 108 (2012) 056802;
Q. Shifei, C. Hua, X. Xiaohong, Z. Zhenyu, Carbon 61 (2013) 609;
C. Bai, X. Zhang, Phys. Rev. B 76 (2007) 075430;
C. Bai, X. Zhang, Phys. Lett. A 372 (2008) 725;
C. Bai, Y. Yang, X. Zhang, Appl. Phys. Lett. 92 (2008) 102513;
C. Bai, Y. Yang, X. Zhang, Phys. Rev. B 80 (2009) 235423.
[22] J.G. Zhu, C. Park, Matter. Today 8 (2006) 35.
[23] T. Yokoyama, Phys. Rev. B 87 (2013) 241409(R).
[24] M. Ezawa, Phys. Rev. Lett. 109 (2012) 055502.
[25] E. Scalise, M. Houssa, G. Pourtois, B. Broek, V. Afanasev, A. Stesmans, Nano Res. 6 (2013) 19.
[26] H.P. Li, R.Q. Zhang, EPL 99 (2012) 36001.
[27] M. Hu, X. Zhang, D. Poulikakos, Phys. Rev. B 87 (2013) 195417.
[28] Q.-X. Pei, Y.-W. Zhang, Z.-D. Sha, V.B. Shenoy, J. Appl. Phys. 114 (2013) 033526.
[29] T.Y. Ng, J. Yeo, Z. Liu, Int. J. Mech. Mater. Des. 9 (2013) 105.
[30] R.K. Pathria, Statistical Mechanics, Oxford Press, London, 1997.
[31] N. Tombros, B. Jo, J. van Wees, Nature (London) 448 (2007) 571.
[32] G. Gui, J. Li, J. Zhong, Phys. Rev. B 78 (2008) 075435.
[33] V.M. Pereira, A.H. Castro Neto, N.M.R. Peres, Phys. Rev. B 80 (2009) 045401.
[34] S.-M. Choi, S.-H. Jhi, Y.-W. Son, Phys. Rev. B 81 (2010) 081407(R).
[35] M. Farjam, H. Rafii-Tabar, Phys. Rev. B 80 (2009) 167401.
[36] G. Liu, M.S. Wu, C.Y. Ouyang, B. Xu, Europhys. Lett. 99 (2012) 17010.
[37] Y. Wang, Y. Ding, Solid State Commun. 155 (2013) 6.
[38] T.P. Kaloni, Y.C. Cheng, U. Schwingenschlogl, J. Appl. Phys. 113 (2013) 104305.
[39] B. Mohan, A. Kumar, P.K. Ahluwalia, Physica E 61 (2014) 40.

[40] H. Zhao, Phys. Lett. A 376 (2012) 3546.
[41] B. Aufray, A. Vizzini, H. Oughaddou, C. Lndri, B. Ealet, G.L. Lay, Appl. Phys. Lett. 96 (2010) 183102.
[42] C.L. Kane, E.J. Mele, Phys. Rev. Lett. 95 (2005) 146802.
[43] C.L. Kane, E.J. Mele, Phys. Rev. Lett. 95 (2005) 226801.
[44] C.J. Tabert, E.J. Nicol, Phys. Rev. B 88 (2013) 085434.
[45] V.M. Pereira, A.H. Castro Neto, N.M.R. Peres, Phys. Rev. B 80 (2009) 045401.
[46] B. Wang, J. Wu, X. Gu, H. Yin, Y. Wei, R. Yang, M. Dresselhaus, Appl. Phys. Lett. 104 (2014) 081902.
[47] L. Chen, B.J. Feng, K.H. Wu, Appl. Phys. Lett. 102 (2013) 081602.

[48] H. Haugen, D. Huertas-Hernando, A. Brataas, Phys. Rev. B 77 (2008) 115406.
[49] Z. Qiao, S.A. Yang, W. Feng, W.-K. Tse, J. Ding, Y. Yao, J. Wang, Q. Niu, Phys. Rev. B 82 (2010) 161414.
[50] M. Yarmohammadi, AIP Adv. 6 (2016) 085008.
[51] C. Kittle, Introduction to Solid State Physics, eighth ed., Wiley, New York, 2004.
[52] X. Xu, J. Chen, B. Li, J. Phys. Condens. Matter. 28 (2016) 483001.
[53] A. Tari, The Specific Heat of Matter at Low Temperatures (Imperial College Press) page 250, 2003.
[54] C. Yesilurt et al., Appl. Phys. Exp. 8 (2015) 105201.